Miniaturized Dual-Band Hybrid Couplers With Arbitrary Power Division Ratios

Ching-Luh Hsu, Jen-Tsai Kuo, *Senior Member, IEEE*, and Chin-Wei Chang

***Abstract*—Branch-line and rat-race couplers are designed to have dual-band operation with arbitrary power division ratios. An elementary two-port is proposed to imitate the 90° section at the two designated frequencies with different characteristic impedances. The two-port consists of a stepped-impedance section with open stubs attached to its two ends, and its circuit parameters are determined by the transmission line theory. The use of the stepped-impedance sections also leads to circuit miniaturization. By the standard microstrip technology, investigated also includes the realizable power division ratios and circuit bandwidths in the two bands, the upper limit of the ratio of the two designated frequencies and the miniaturization factor of the proposed circuit. Hybrid couplers operating at 2.45/5.2 GHz with various power division ratios are designed, fabricated and tested. Experiment results are compared with the theory and simulation.**

***Index Terms*—Branch-line coupler, dual band, miniaturization, rat-race coupler, stepped impedance.**

I. Introduction

DESIGN OF multiband RF circuits has become an important research topic due to recent rapid development of mobile and wireless communications. Existing examples of dual-band systems include the GSM 900/1800 cellular phone and the 802.11a/b wireless local area network (WLAN). For saving cost, multiband components are usually required in the RF parts of these systems. Obviously, a single circuit operating at multiple bands is of particular interest since it uses a smaller circuit area and possibly possesses lower insertion loss.

Hybrid couplers are one of the most important passive microwave devices. In the past, several approaches have been proposed for design of dual-band hybrid couplers [1]–[8]. In [1] and [2], the quarter-wave $(\lambda/4)$ sections of the conventional coupler are replaced by composite right/left-handed transmission lines. In their realization, however, significant losses are caused by the lumped elements and via-holes in the assembly of left-handed transmission lines. In [3] and [4], a straight line section loaded with a shunt element is proposed to play the role of a $\lambda/4$ section in a conventional hybrid for dual-band purpose. The design is based on the equivalence of the $ABCD$ matrices of the two elementary two-ports at the two designated frequencies. The cross-coupled [5] and the three structures in [6] can also be used to implement dual-band quadrature couplers. In [7], a hybrid-ring loaded with two identical short-circuited stubs is proposed to realize the dual-band performance. In [8], a rat-race coupler operating at two widely separated frequencies is devised with a compact size and low insertion loss.

It has been shown in [9]–[12] that hybrid couplers may have arbitrary output power division by controlling the characteristic impedances of the $\lambda/4$ sections. The purpose of this paper is to extend their formulations to develop dual-band branch-line and rat-race couplers with arbitrary power divisions at the two designated bands. These couplers will be useful for dual-band mixers and antenna arrays.

For rat-race and branch-line couplers, miniaturization is of particular interest since the conventional circuits has a circumference of 1λ or $3\lambda/2$. Multifolded traces [13] and fractal-line sections [14] and patterned ground structures [15] are possible ways to miniaturize the circuits. In [16], the area reduction is achieved by line sections loaded with several equally separated open stubs. In [17], a periodic stepped-impedance ring is designed to shrink the size of a rat-race coupler by more than 75%. In [18], the dual-band 2.45/5.2 GHz rat-race coupler with equal power division uses only 21% of the area of a conventional circuit at the first band. The circuits proposed here also provide good size reduction factors, and this will be discussed latter.

This paper is organized as follows. In Section II, design equations for single-band hybrid couplers with arbitrary power division are briefly reviewed. These equations are extended in Section III to perform the dual-band operation. Design graphs for such dual-band branch-line and rat-race couplers are demonstrated in Sections IV and V, respectively. The constraint of the design imposed by the line width resolution in microstrip realization is also investigated. Measurement and simulation results of some experimental circuits are presented in Sections VI, and a conclusion is drawn in VII.

II. Hybrid Couplers With Arbitrary Power Division for Single-Band Operation

Fig. 1 shows the circuit schematics of the two hybrid couplers with arbitrary power division. For a branch-line hybrid with $|S_{21}| - |S_{31}| = \Delta\ (dB)$ and $d = 10^{\Delta/20}$, the characteristic impedances Z_α and Z_β are given as [10], [11]

$$\frac{Z_\beta}{Z_0} = d \tag{1}$$

Manuscript received February 11, 2008; revised October 02, 2008. First published December 12, 2008; current version published January 08, 2009. This work was supported in part by the Ministry of Education under the ATU Program and by the National Science Council, Taiwan, under Grant NSC 95-2752-E-009-003-PAE, Grant NSC 95-2221-E-009-037-MY2, and Grant NSC 96-2221-E-009-245.

C.-L. Hsu was with Department of Communication Engineering, National Chiao Tung University, Hsinchu, 300 Taiwan. He is now with the Department of Electronic Engineering, Ta Hwa Institute of Technology, Hsinchu, 307 Taiwan.

J.-T. Kuo and C.-W. Chang are with the Department of Communication Engineering, National Chiao Tung University, Hsinchu, 300 Taiwan (e-mail: jtkuo@mail.nctu.edu.tw).

Color versions of one or more of the figures in this paper are available online at http://ieeexplore.ieee.org.

Digital Object Identifier 10.1109/TMTT.2008.2009036

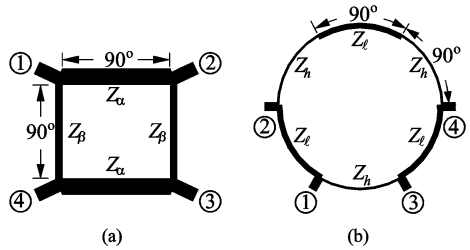

Fig. 1. Circuit schematics of: (a) branch-line coupler and (b) rat-race coupler with arbitrary power division for single-band operation.

$$\frac{Z_\alpha}{Z_0} = \frac{d}{\sqrt{1+d^2}} \tag{2}$$

where Z_0 is the system impedance. The rat-race ring in Fig. 1(b) has six $\lambda/4$ sections with alternative characteristic impedances Z_l and Z_h to achieve an arbitrary power division [12]. The power division ratio is $|S_{21}| - |S_{31}| = |S_{34}| - |S_{24}| = \Delta(\text{dB})$ and is related to Z_l and Z_h by

$$\Delta = 20\log\frac{2Z_h^2}{Z_\ell\,(Z_h + Z_\ell)}. \tag{3}$$

In synthesis, when the power division $\Delta = 10\log(d^2)$ is given, Z_l and Z_h can be expressed as

$$Z_h = Z_0\sqrt{S^2 + \frac{1}{S}} \tag{4}$$

$$Z_\ell = \frac{Z_h}{S} \tag{5}$$

$$S = \frac{d}{4}\left(1 + \sqrt{1 + \frac{8}{d}}\right). \tag{6}$$

One can see from (1) and (2) for the branch-line coupler and (4)–(6) for the rat-race coupler, that once d (or Δ) is given, there is no degree of freedom in choosing the design parameters for the circuits in Fig. 1.

III. Elementary Two-Port for Dual-Band Operation

Both the hybrids in Fig. 1 consist of several $\lambda/4$ sections at the design frequency. The admittance matrix of such a section with characteristic impedance Z_T can be written as

$$Y_{\lambda/4} = \begin{bmatrix} 0 & j\left(\dfrac{1}{Z_T}\right) \\ j\left(\dfrac{1}{Z_T}\right) & 0 \end{bmatrix}. \tag{7}$$

The elementary two-port in Fig. 2 is proposed to imitate the $\lambda/4$ sections to our purpose. It consists of two identical high-Z segments on both sides and a low-Z segment in the middle. In addition, two shunt elements are attached to the ends of the two-port. This two-port has to imitate an electric length of 90° and different equivalent characteristic impedances at the two designated frequencies (denoted as f_1, f_2, and $f_2/f_1 \equiv n$) to perform the dual-band operation. The design is as follows. Let $R = Z_a/Z_b > 1$ be the impedance ratio of the section. To

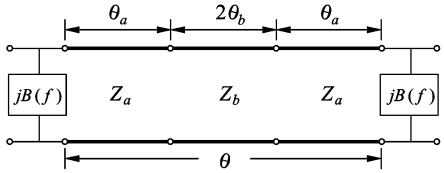

Fig. 2. Elementary two-port for design of dual-band hybrids.

facilitate the derivation of the Y-matrix of the two-port in Fig. 2, one can utilize the symmetry of the network [18]. If the imitated characteristic impedances (Z_T) at f_1 and f_2 are, respectively, Z_1 and Z_2, one can validate that

$$Z_1 = \frac{2Z_a}{P(\theta_a,\theta_b) - Q(\theta_a,\theta_b)} \tag{8a}$$

$$Z_2 = \frac{2Z_a}{P(n\theta_a,n\theta_b) - Q(n\theta_a,n\theta_b)} \tag{8b}$$

where

$$P(\theta_a,\theta_b) = \frac{\tan\theta_a + R\tan\theta_b}{1 - R\tan\theta_a\tan\theta_b} \tag{8c}$$

$$Q(\theta_a,\theta_b) = \frac{\tan\theta_a\tan\theta_b - R}{R\tan\theta_a + \tan\theta_b} \tag{8d}$$

and θ_a and θ_b are evaluated at f_1. The functions $P(\theta_a,\theta_b)$ and $Q(\theta_a,\theta_b)$ are directly related to the input admittances of the network in Fig. 2 when its symmetric plane is open and short circuited, respectively. Enforcing the diagonal terms of the Y-matrix of the two-port to zero, we have the shunt susceptance

$$B(\theta_a,\theta_b) = -\frac{P(\theta_a,\theta_b) + Q(\theta_a,\theta_b)}{2Z_a}. \tag{9}$$

Since both the hybrids in Fig. 1 are closed structures, the two shunt susceptances at each impedance junction can be merged together and implemented by a single open stub. Let θ_s be the length at f_1 and Z_s be the characteristic impedance of the stub. Then the susceptances of the stub at f_1 and f_2 are $\tan\theta_s/Z_s$ and $\tan n\theta_s/Z_s$. For branch-line couplers, the length θ_s can be obtained by [18]

$$\frac{B_\alpha(\theta_a,\theta_b) + B_\beta(\theta_a,\theta_b)}{B_\alpha(n\theta_a,n\theta_b) + B_\beta(n\theta_a,n\theta_b)} = \frac{\tan\theta_s}{\tan n\theta_s} \tag{10}$$

where the subscripts α and β denote the shunt susceptances for imitating the $\lambda/4$ sections with Z_α and Z_β in Fig. 1(a), respectively. The characteristic impedance of the stub Z_s can then be calculated by

$$Z_s = \frac{\tan\theta_s}{B_\alpha(\theta_a,\theta_b) + B_\beta(\theta_a,\theta_b)}. \tag{11}$$

For the dual-band rat-race coupler, the characteristic impedances Z_l and Z_h and the shunt susceptance can be determined in a similar fashion. Given Z_0 and the power division (in decibels) Δ_1 at f_1 and Δ_2 at f_2, values of Z_1 and Z_2 can be known. Define

$$M = \frac{Z_2}{Z_1} = \frac{P(\theta_a,\theta_b) - Q(\theta_a,\theta_b)}{P(n\theta_a,n\theta_b) - Q(n\theta_a,n\theta_b)}. \tag{12}$$

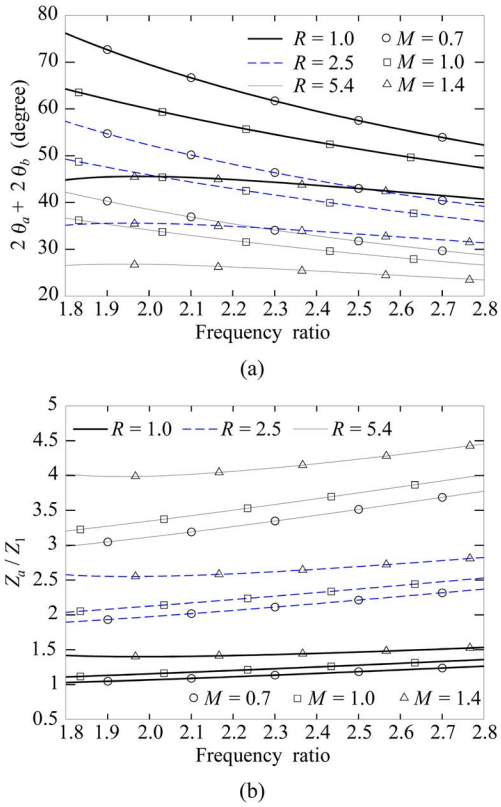

Fig. 3. (a) Branch length and (b) Z_a/Z_1 against the frequency ratio $n = f_2/f_1$ for various values of M and R.

If $R = 1$ is chosen, (12) can be reduced to

$$M = \frac{\sin n\theta}{\sin \theta} \tag{13}$$

which can be used to solve the total length $\theta = 2(\theta_a + \theta_b)$. Fig. 3(a) plots the values of θ against the frequency ratio $1.8 \le n \le 2.8$ for various M and R values with $\theta_a = \theta_b$, which is an approximate solution for minimizing θ[17]. Since $\theta < 90°$ for all the case studies, sections with $R > 1$ can be used for size reduction. Furthermore, the larger the M value is, the smaller the lengths of the branches are. Obviously, the branch lengths can also be saved due to the shunt elements jB [19]. It can be validated that such dual-band coupler has an area reduction factor of $(2\theta/\pi)^2$ for operation at f_1. Note that when $M = 1$, i.e., the power divisions in the two designated bands are identical, it can be derived that $\theta = \pi/(1 + n)$ [18] and the area reduction factor is $[2/(1 + n)]^2$, in comparison with the conventional circuit at f_1. Fig. 3(b) plots Z_a/Z_1 ratios for all case studies in Fig. 3(a). It indicates that the characteristic impedances of the branch lines of the dual-band hybrid are higher than those of a single-band counterpart. Note that by the standard microstrip process, the Z_a value has an upper realizable limit, and so do R and M. Thus, the degree of miniaturization and the power division of our proposed circuits cannot be arbitrary. This point will be investigated below.

IV. Dual-Band Branch-Line Coupler With Arbitrary Power Divisions

Let Δ_1 and Δ_2 be, respectively, the power division ratios at f_1 and f_2 in decibels. For a dual-band branch-line coupler, the required values of Z_α and Z_β at the two frequencies can be calculated by (1) and (2). By choosing $R = 1$ and merging the adjacent shunt open stubs, the final circuit layout is shown in Fig. 4. In this study, let $f_1 = 2.4$ GHz and $f_2 = 5.2$ GHz.

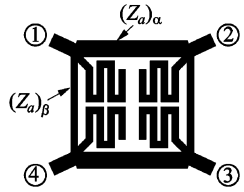

Fig. 4. Circuit layout of a dual-band branch-line coupler with arbitrary power division ratios.

For $n = 1.8, 2.1$, and 2.8 and $\Delta_2 = \Delta_1 - 3$, Δ_1, and $\Delta_1 + 3$ (dB), Fig. 5(a) plots the normalized characteristic impedances of the branches and Fig. 5(b) plots that of the shunt open stub against the power division ratio in decibels. First consider the design with $R = 1(Z_a = Z_b)$ and $M = 1(\Delta_1 = \Delta_2 \equiv \Delta)$. The characteristic impedances of the section in Fig. 2 for imitating the Z_α and Z_β sections can be simply expressed as

$$\frac{(Z_a)_\alpha}{Z_0} = \frac{d}{\sqrt{1+d^2}} \csc \frac{\pi}{1+n} \tag{14}$$

$$\frac{(Z_a)_\beta}{Z_0} = d \csc \frac{\pi}{1+n}. \tag{15}$$

From (10), $\theta_s = \pi/(1 + n)$, and from (11),

$$\frac{Z_s}{Z_0} = \frac{d}{1+\sqrt{1+d^2}} \frac{\sin(\theta_s)}{\cos^2(\theta_s)}. \tag{16}$$

In our microstrip fabrication process, the characteristic impedance of the minimal line width is about 150 Ω for a substrate with $\epsilon_r = 2.2$ and thickness $= 0.508$ mm. Thus, the normalized impedances $(Z_a)_\alpha/Z_0$, $(Z_a)_\beta/Z_0$, and Z_s/Z_0 must be no more than 3.0 when $Z_0 = 50\ \Omega$. As shown in Fig. 5(a), the upper limit of Δ is decreased approximately linearly from 8.6 to 6.4 dB when n is increased from 1.8 to 2.8. In Fig. 5(b), $Z_s < 150\ \Omega$ can be obtained when $n = 1.8$ for $\Delta \le 6.3$ dB.

If $\Delta_1 \neq \Delta_2$, (12) can be invoked as the first step to calculate the circuit parameters. For example, $\Delta_1 = 3$ dB at $f_1 = 2.45$ GHz and $\Delta_2 = 6$ dB at $f_2 = 5.2$ GHz. From (1) and (2), it can be validated that $Z_\alpha = 40.8$ and $44.7\ \Omega$ and $Z_\beta = 70.6$ and $99.8\ \Omega$ at f_1 and f_2, respectively. The value of M in (12) are then set to $44.7/40.8 = 1.095$ and $99.8/70.6 = 1.413$ for imitating the $(Z_a)_\alpha$ and $(Z_a)_\beta$ sections, respectively. As indicted in Fig. 5(a), the values of $(Z_a)_\alpha$ and $(Z_a)_\beta$ are 50 and 100 Ω, and from (13), their lengths at f_1 are 54.84° and 44.84°, respectively. Based on (10), the parameters for the shunt stubs are $Z_s = 86.34\ \Omega$ and $\theta_s = 64.4°$. When $n = 2.8$, Fig. 5(a) shows that the upper limits for realizable power division ratios for Δ_1 are 7.5, 6.4, and 5.8 dB when $\Delta_2 = \Delta_1 - 3$, $\Delta_2 = \Delta_1$, and $\Delta_2 = \Delta_1 + 3$, respectively.

V. Dual-Band Rat-Race Coupler With Arbitrary Power Divisions

Fig. 6 shows the layout of the dual-band rat-race coupler with $R > 1$. Each of the six interlaced quarter-wave Z_l or Z_h sections in Fig. 1(b) will be replaced by the elementary

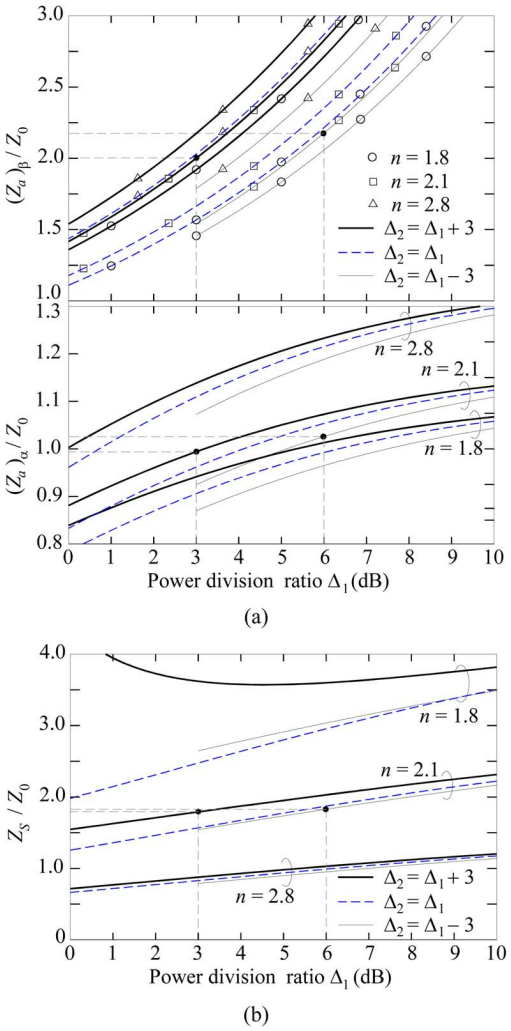

Fig. 5. Normalized characteristic impedances against power division ratio for the dual-band branch-line coupler with $R = 1$ for various n. (a) Z_α and Z_β sections. (b) Z_s/Z_0.

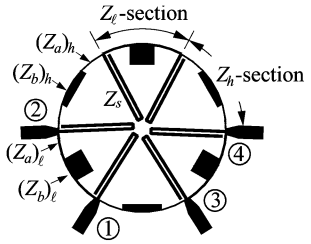

Fig. 6. Circuit layout of the dual-band rat-race coupler with arbitrary power division ratios.

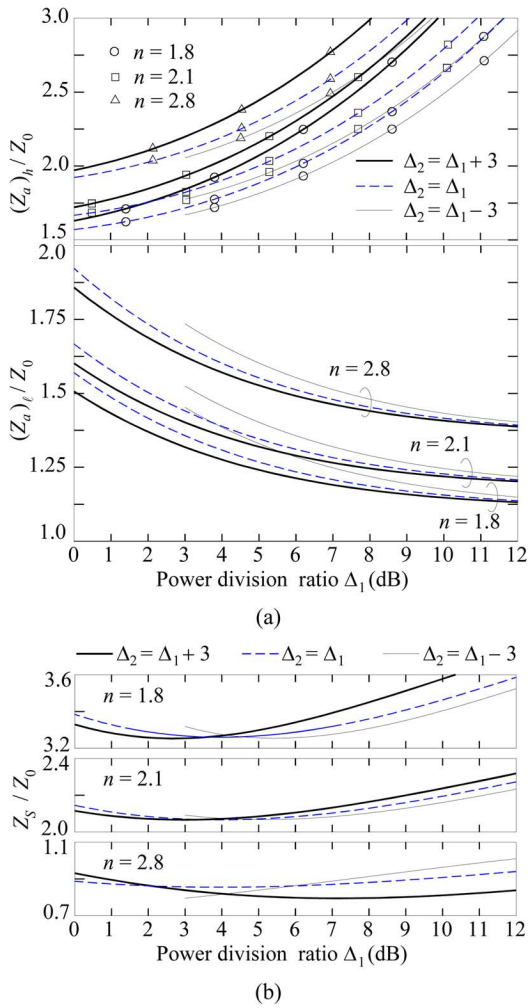

Fig. 7. Normalized characteristic impedance against power division ratio for the rat-race coupler for various n. (a) Z_l/Z_0 and Z_h/Z_0. (b) Z_s/Z_0.

two-port in Fig. 2. The realizable power division ratio limit of the rat-race coupler is investigated as follows. Let $(Z_a)_l$ and $(Z_a)_h$, respectively, denote the characteristic impedances of the stepped-impedance section in Fig. 2 for the Z_l and Z_h sections in Fig. 1(b). The value of Z_a can be determined by (8a) once $P(\theta_a, \theta_b)$ and $Q(\theta_a, \theta_b)$ are known. Fig. 7(a) plots $(Z_a)_l$ and $(Z_a)_h$ and Fig. 7(b) plots Z_s/Z_0 of the shunt stub against Δ_1 for various n when the stepped-impedance section has $R = 1$. When $n = 2.1$, it can be seen that the upper limit of Δ is 11 dB, and that $Z_s/Z_0 > 3$ when $n = 1.8$ for $\Delta_2 = \Delta_1 - 3$, $\Delta_2 = \Delta_1$, and $\Delta_2 = \Delta_1 + 3$.

For investigating the size reduction factor with $R \geq 1$, Fig. 8(a) and (b), respectively, plot $\theta_a + \theta_b$ and Z_a/Z_1 against θ_b for various R values when $n = 2.12$ (e.g., $f_1 = 2.45$ GHz and $f_2 = 5.2$ GHz) and $M = 1(\Delta_1 = \Delta_2 = \Delta)$. When $R = 1$, $\theta_a + \theta_b = 28.83°$, as shown via the horizontal dashed line in Fig. 8(a). When $R > 1$, each $\theta_a + \theta_b$ curve has a minimum and it decreases as R is increased. When $R > 3$, it is found that the condition of the minimum can be approximated by $\theta_a = \theta_b$. Fig. 8(b) indicates that $Z_a/Z_1 = 1.18$ for $R = 1$. For the circuit with $\Delta = 0$ dB and $R = 1$, the characteristic impedance $Z_a = 1.18 \times \sqrt{2}\, Z_0 = 83.4\ \Omega$. From (19) and (20), when $\Delta = 6$ dB, $Z_h = 89.8\ \Omega$, and $Z_l = 55.6\ \Omega$, then $(Z_a)_h = 106\ \Omega$ and $(Z_a)_l = 65.6\ \Omega$. In Fig. 8(b), it is noted that each Z_a/Z_1 curve increases monotonically when either θ_b or R is increased if $R > 1$.

As indicated in Fig. 8(a), more circuit miniaturization can be achieved by using $R > 1$. It is found however, that Z_a/Z_1 also increases at the same time when R is increased. It means that the size reduction factor has an upper limit. For the Z_l section, Fig. 8(b) shows that its Z_a/Z_1 ratio must be no more than 2.12, 2.455, and 2.698 when $\Delta_1 = \Delta_2 = 0$ dB ($Z_l = 70.7\ \Omega$), 3 dB ($Z_l = 61.1\ \Omega$), and 6 dB ($Z_l = 55.6\ \Omega$), respectively, as

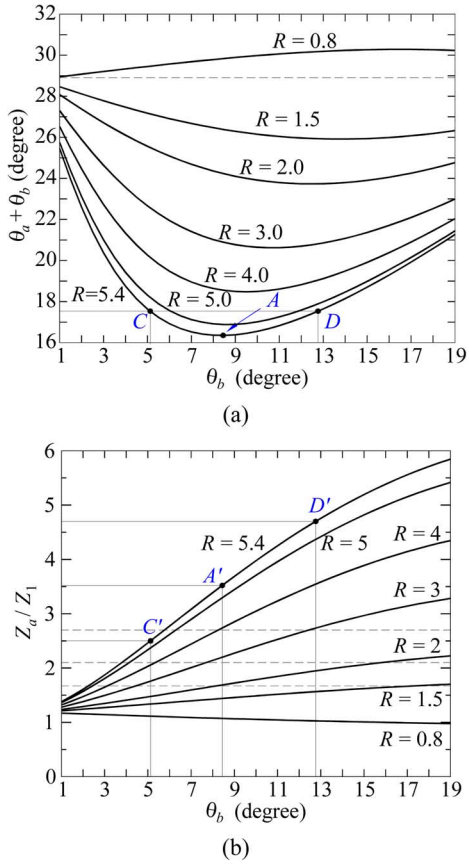

Fig. 8. Solutions for the circuit with $\Delta_1 = \Delta_2$ and $n = 2.12$. (a) $\theta_a + \theta_b$. (b) Z_a/Z_1.

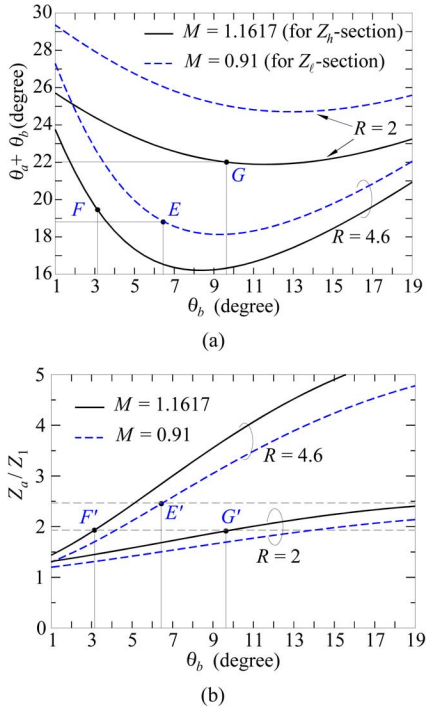

Fig. 9. Solutions for the circuit with $n = 2.12$, $\Delta_1 = 3$ dB, and $\Delta_2 = 6$ dB. (a) $\theta_a + \theta_b$. (b) Z_a/Z_1.

indicated by the three horizontal dashed lines. If $\Delta_1 = \Delta_2 = 6$ dB and $R = 5.4$, it can be found that θ_b is about 8.4° to achieve the minimal length, as shown by point A. Point A' in Fig. 8(b), however, indicates that such value of $(Z_a)_l$ is forbidden since $Z_a/Z_1 = 3.5 > 2.12$. We can increase $\theta_a + \theta_b$ from 16.8° to 17.5° for reducing $(Z_a)_l$. When $\theta_a + \theta_b = 17.5°$, there are two possible solutions as indicated by points C and D. Only the design with the smaller θ_b (point C or C') is feasible since the $(Z_a)_l$ value at point D (or D') is not realizable. Detailed data show that the Z_l section (point C) length is 60% of that for $R = 1$. The size reduction of the Z_h section in Fig. 6 can be done in a similar fashion.

When the coupler has $\Delta_1 = 3$ dB and $\Delta_2 = 6$ dB, it is necessary to solve (12) with $M = 1.1617$ and 0.91 for the Z_h and Z_l section, respectively. It can be validated that $Z_h = 77.3\ \Omega$ and 89.8 Ω and $Z_l = 61.1\ \Omega$ and 55.6 Ω at $f = f_1$ and f_2, respectively. Fig. 9(a) and (b) plot the results for $\theta_a + \theta_b$ and Z_a/Z_1 against θ_b for $R = 2$ and 4.6. Note that the $\theta_a + \theta_b$ solution is decreased when M increases for a given R. In Fig. 9(b), the horizontal dashed lines show the borderlines of forbidden regions for miniaturizing the Z_l and Z_h section of the coupler with $\Delta_1 = 3$ dB and $\Delta_2 = 6$ dB. For the Z_l section, it is possible to realize the following parameters: $\theta_a = 12.32°$, $\theta_b = 6.5°$, $R = 4.6$, and $Z_a = 150\,\Omega$ (point E'). Thus, the length of the Z_l section is reduced by a factor of $18.82/30.11 = 37.5\%$ (point E). For the Z_h section, however, $R = 4.6$ is not adequate for a substrate with $\epsilon_r = 2.2$ and 0.508-mm thickness because the solution of θ_b is only 3° when $Z_a = 150\ \Omega$ (point F') since it is not practical to implement such a short section with a large width. In Fig. 9(b), point G' indicates the realizable Z_a/Z_1 for Z_h section when $R = 2$ and $Z_a = 150\ \Omega$. In this way, however, the total length of Z_h section can be reduced by only 17%. Fortunately, for the coupler with $\Delta_1 < \Delta_2$, the Z_h section tends to have a shorter length than the Z_l section for the same R value. On the contrary, the Z_h section will be longer than the Z_l section when the coupler has $\Delta_1 > \Delta_2$ for the same R value.

TABLE I
CIRCUIT PARAMETERS OF THE TWO EXPERIMENTAL DUAL-BAND BRANCH-LINE COUPLERS

Coupler	Δ_1	Δ_2	Z_a-section		Z_β-section		Stub	
			θ	$Z_a(\Omega)$	θ	$Z_a(\Omega)$	θ_s	$Z_s(\Omega)$
A	3	6	54.8°	50.0	44.8°	100	64.4°	86.3
B	6	3	60.1°	51.5	65.8°	109	53.5°	88.6

VI. SIMULATION AND MEASUREMENT

In the following, the two operation frequencies of all experimental hybrids are 2.45 and 5.2 GHz. Two branch-line and three rat-race couplers are fabricated and measured. The circuit parameters and the circuit bandwidths are listed in Tables I and II, respectively. The bandwidths are measured by the frequencies where $|S_{11}| = -15$ dB, $|S_{41}| = -15$ dB, $|S_{21}|/|S_{31}| - \Delta_i = \pm 0.5$ dB, and $\angle S_{31} - \angle S_{21} + 90° = \pm 5°$. The counterparts of the three rat races are in Tables III and IV. For simplicity, only one circuit is chosen from each type of the coupler to compare the measured data with simulation. All simulations are carried out by the full-wave software package IE3D [20].

The first branch-line coupler (Coupler A) is designed to have $\Delta_1 = 3$ dB and $\Delta_2 = 6$ dB using $R = 1$. Fig. 10(a) com-

TABLE II
BANDWIDTHS (%) OF THE TWO EXPERIMENTAL DUAL-BAND BRANCH-LINE COUPLERS

Coupler		$\lvert S_{21}\rvert/\lvert S_{31}\rvert$ ($\Delta_i \pm 0.5$ dB)	$\angle S_{31} - \angle S_{21}$ (-90 ± 5°)	$1/\lvert S_{11}\rvert$ (> 15 dB)	$1/\lvert S_{41}\rvert$ (> 15 dB)
A	Sim.	11.1/14.3	23.3/24.3	16.6/23	13.7/15.1
	Meas.	10.5/15.1	21.5/22.3	15.5/23.5	14.1/15.5
B	Sim.	19.7/5.29	41.9/8.96	37.6/7.1	25.5/5.95
	Meas.	18.0/5.5	40.2/9.5	35.4/6.8	24.3/5.5

TABLE III
CIRCUIT PARAMETERS OF THE THREE EXPERIMENTAL DUAL-BAND RAT RACES

Coupler	Δ_1	Δ_2	Z_h-section		Z_ℓ-section		Stub	
			θ_a/θ_b	Z_a/Z_b (Ω)	θ_a/θ_b	Z_a/Z_b (Ω)	θ_s	Z_s(Ω)
C	6	3	16.3°/9.4°	150/74	9.41°/9.4°	150/44.1	64.2°	108.5
D	3	6	12.4°/9.42°	150/72.6	12.4°/6.43°	150/32.6	65.1°	105.6
E	6	6	18.8°/5.13°	145/58	12.4°/5.13°	139/25.7	64.3°	108

TABLE IV
BANDWIDTHS (%) OF THE THREE EXPERIMENTAL DUAL-BAND RAT RACES

Coupler		$\lvert S_{21}\rvert/\lvert S_{31}\rvert$ ($\Delta \pm 0.5$ dB)	$\angle S_{31} - \angle S_{21}$ (±5°)	$\angle S_{24} - \angle S_{34}$ (180° ± 5°)	$1/\lvert S_{11}\rvert$ (> 15 dB)	$1/\lvert S_{41}\rvert$ (> 15 dB)
C	Sim.	17.1/5.2	7.8/5.0	9.8/6.5	30/12.5	42/16.5
	Meas.	16.3/5.1	7.2/5.0	10/6.0	28.6/12	39./15.5
D	Sim.	11.8/12.9	7.8/5.7	9.5/7.1	24.1/14	29/17.2
	Meas.	11.5/12.1	7.0/5.5	9.0/6.8	25/13.2	31/16.0
E	Sim.	13.6/11	7.7/5.9	9.4/7.1	29.6/9.1	48.9/9.5
	Meas.	14/10.5	7.2/5.5	9.0/6.7	27.8/8.3	45/9.0

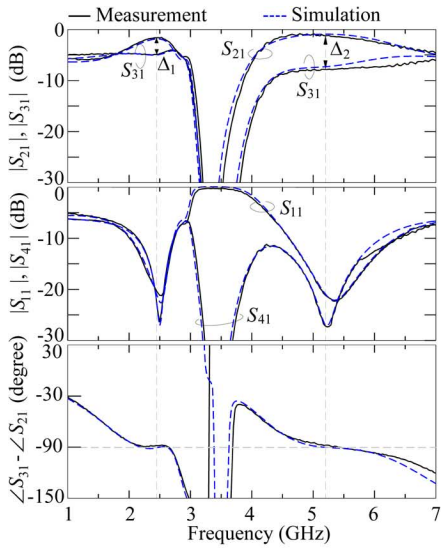

(a)

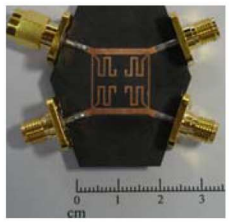

(b)

Fig. 10. Performances of 2.45/5.2-GHz branch-line coupler (Coupler A) with $\Delta_1 = 3$ dB and $\Delta_2 = 6$ dB. (a) $|S_{11}|$, $|S_{21}|$, $|S_{31}|$, $|S_{41}|$, and $\angle S_{31} - \angle S_{21}$. (b) Photograph of the fabricated circuit.

pares the measured responses of $|S_{21}|$, $|S_{31}|$, $|S_{11}|$, $|S_{41}|$, and $\angle S_{31} - \angle S_{21}$ with the simulation data. The measurement shows that at $f_1 = 2.45$ GHz, $|S_{11}| = -20.7$ dB, $|S_{21}| = -1.07$ dB, $|S_{31}| = -4.23$ dB ($\Delta_1 = 3.16$ dB), and $|S_{41}| = -24.6$ dB, and at $f_2 = 5.2$ GHz, $|S_{11}| = -22.1$ dB, $|S_{21}| = -0.88$ dB, $|S_{31}| = -7.68$ dB ($\Delta_2 = 6.8$ dB), and $|S_{41}| = -27.2$ dB. The error of Δ_2 (0.8 dB) could be caused by the discontinuities. The measured relative phase deviations $\angle S_{31} - \angle S_{21} + 90°$ at f_1 and f_2 are only 2.2° and 3.1°, respectively. Fig. 10(c) shows the photograph of the experimental circuit. Note that $R = 1$ is chosen for this coupler. The shunt stubs are folded to accommodate the room inside the ring. It is simply due to that the stubs already occupy almost all the space inside the coupler. If $R > 1$ is used, the space inside the circuit will not be sufficient for the stubs, since the stepped-impedance design will shrink the coupler area. On the other hand, if it is designed at a lower frequency, the space can be larger, then the use of $R > 1$, and hence, a better size reduction factor, becomes possible.

The second branch-line coupler (Coupler B) is designed with $\Delta_1 = 6$ dB, $\Delta_2 = 3$ dB, and $R = 1$. Its circuit parameters are listed in Table I. In comparison with Coupler A, the characteristic impedances of the branches and stubs are slightly increased, but the electric lengths have relatively large changes. The simulated and measured fractional bandwidths of couplers A and B are in Table II. For Coupler A, the bandwidths at f_1 and f_2 are of the same order, but for Coupler B, the relative bandwidths at f_1 are much larger than those at f_2. The measured data have good agreement with the simulation.

The first experimental rat-race coupler (Coupler C) is designed to have $\Delta_1 = 6$ dB and $\Delta_2 = 3$ dB. The shunt open stub has $\theta_s = 64.2°$ and $Z_s = 108.5\ \Omega$. Fig. 11(a) plots the simulation and measured responses of $|S_{11}|$, $|S_{21}|$, $|S_{31}|$, and $|S_{41}|$. The measurement shows that at f_1, $|S_{11}| = -21.4$ dB, $|S_{21}| = -1.29$ dB, $|S_{31}| = -7.36$ dB ($\Delta_1 = 6.07$ dB), and $|S_{41}| = -22.5$ dB, and at f_2, $|S_{11}| = -15.8$ dB, $|S_{21}| = -2.32$ dB, $|S_{31}| = -5.3$ dB ($\Delta_2 = 2.98$ dB), and $|S_{41}| = -22.5$ dB. Note that Δ_1 and Δ_2 have been accurately implemented. Fig. 11(b) plots the phase differences $\angle S_{31} - \angle S_{21}$ and $\angle S_{24} - \angle S_{34}$, respectively. The measured data show that the relative phase deviations $\angle S_{31} - \angle S_{21}$ are 1.3° and 2.4° and $\angle S_{24} - \angle S_{34} + 180°$ are 1.8° and 2.1° at f_1 and f_2, respectively. The simulation and experiment results have good agreement all over the band of interest. Fig. 11(c) shows a photograph of the measured rat race.

The second dual-band rat-race coupler (Coupler D) has $\Delta_1 = 3$ dB and $\Delta_2 = 6$ dB, and the third one (Coupler E) has $\Delta_1 = \Delta_2 = 6$ dB. The characteristic impedances and electric lengths at f_1 of the arms and shunt stubs are summarized in Table III. Note that the parameters of Coupler D can also be referred to points G and G' in Fig. 9. There is one degree of freedom in solving (8a) and (8b) when $R \neq 1$. We enforce $Z_a = 150\ \Omega$ in design of Couplers C and D. However, in design of Coupler E, we enforce $\theta_b = 5.13°$. The total circumference of Couplers C, D, and E are only 267.1°, 243.9°, and 248.8° so that the circuits use only 24.5%, 20.4% and 21.2%, respectively, of the area of a conventional circuit at f_1.

The simulation and measured bandwidths of the three experimental rat races are listed in Table IV. Obviously, the band-

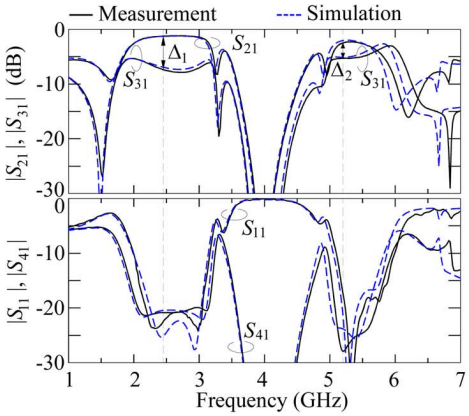

(a)

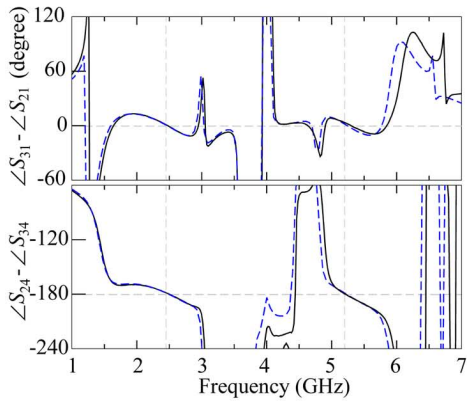

(b)

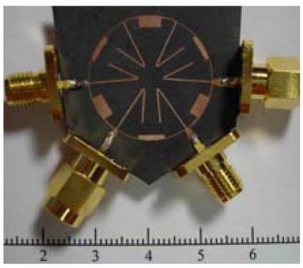

(c)

Fig. 11. Performances of the 2.45/5.2-GHz rat-race coupler (Coupler C). (a) $|S_{11}|$, $|S_{21}|$, $|S_{31}|$ and $|S_{41}|$. (b) $\angle S_{31} - \angle S_{21}$, and $\angle S_{24} - \angle S_{34}$. (c) Photograph of the fabricated circuit.

widths of the circuit at the two operating frequencies are much smaller than those of the conventional single-band circuit. In general, the bandwidths measured by relative phase deviation 5° are smaller than those by $|S_{11}| = -15$ dB and $|S_{41}| = -15$ dB, and the bandwidths of the couplers at f_1 are wider than those at f_2, except for coupler D of which the bandwidth of the amplitude unbalance $|S_{21}|/|S_{31}|$ at 5.2 GHz is slightly wider than that at 2.45 GHz. All measured data have good agreement with the simulation results.

VII. Conclusion

Design technique for dual-band branch-line and rat-race couplers with arbitrary output power division ratios has been presented. An elementary two-port consisting of a stepped-impedance section with two shunt open stubs is used to imitate the $\lambda/4$ section at two designated frequencies. The parameters of the two-port are determined by formulating the equivalence between the two-port and the imitated section at the designated frequencies. Design graphs are provided for determining circuit parameters. In planar realization, the power division ratio is mainly limited by line width of the high-Z segment of the stepped-impedance section while the frequency ratio is limited by that of the attached open stub. It has been shown that a good miniaturization factor for rat-race couplers can be achieved if a large impedance ratio is chosen. The agreement between the measured data and the simulation results of the experimental circuits validates the theory.

References

[1] I.-H. Lin, M. Devincentis, C. Caloz, and T. Itoh, "Arbitrary dual-band components using composite right/left-handed transmission lines," *IEEE Trans. Microw. Theory Tech.*, vol. 52, no. 4, pp. 1142–1149, Apr. 2004.

[2] X. Q. Lin, R. P. Liu, X. M. Yang, J. X. Chen, X. X. Ying, and Q. Cheng, "Arbitrarily dual-band components using simplified structures of conventional CRLH TLs," *IEEE Trans. Microw. Theory Tech.*, vol. 54, no. 7, pp. 2902–2909, Jul. 2006.

[3] K.-K. M. Cheng and F.-L. Wong, "A novel approach to the design and implementation of dual-band compact planar 90° branch line coupler," *IEEE Trans. Microw. Theory Tech.*, vol. 52, no. 11, pp. 2458–2463, Nov. 2004.

[4] H. Zhang and K. J. Chen, "A stub tapped branch line coupler for dual-band operations," *IEEE Microw. Wireless Compon. Lett.*, vol. 17, no. 2, pp. 106–108, Feb. 2007.

[5] M.-J. Park and B. Lee, "Dual-band cross-coupled branch line coupler," *IEEE Microw. Wireless Compon. Lett.*, vol. 15, no. 10, pp. 655–657, Oct. 2005.

[6] C. Collado, A. Grau, and F. D. Flaviis, "Dual-band planar quadrature hybrid with enhanced bandwidth response," *IEEE Trans. Microw. Theory Tech.*, vol. 54, no. 1, pp. 180–188, Jan. 2006.

[7] K.-K. M. Cheng and F.-L. Wong, "A novel rat race coupler design for dual-band applications," *IEEE Microw. Wireless Compon. Lett.*, vol. 15, no. 8, pp. 521–523, Aug. 2005.

[8] K. K. M. Cheng and F. L. Wong, "Dual-band rat-race coupler design using tri section branch line," *Electron. Lett.*, vol. 43, no. 6, pp. 41–42, Mar. 2007.

[9] C. Y. Pon, "Hybrid-ring directional coupler for arbitrary power division," *IEEE Trans. Microw. Theory Tech.*, vol. MTT-19, no. 11, pp. 529–535, Nov. 1961.

[10] R. Levy and L. J. Lind, "Synthesis of symmetric branch line guide directional couplers," *IEEE Trans. Microw. Theory Tech.*, vol. MTT-16, no. 12, pp. 80–89, Dec. 1968.

[11] G. L. Matthaei, L. Young, and E. M. T. Jones, *Microwave Filters, Impedance-Matching Network, and Coupling Structures*. Norwood, MA: Artech House, 1980, ch. 13.

[12] A. K. Agrawal and G. F. Mikucki, "A printed-circuit hybrid-ring directional coupler for arbitrary power divisions," *IEEE Trans. Microw. Theory Tech.*, vol. MTT-34, no. 12, pp. 1401–1407, Dec. 1986.

[13] R. K. Settaluri, G. Sundberg, A. Weisshaar, and V. K. Tripathi, "Compact folded line rat-race hybrid couplers," *IEEE Microw. Guided Wave Lett.*, vol. 10, no. 2, pp. 61–63, Feb. 2000.

[14] H. Ghali and T. A. Moselhy, "Miniaturized fractal rat-race, branch-line, and coupled-line hybrids," *IEEE Trans. Microw. Theory Tech.*, vol. 52, no. 11, pp. 2513–2520, Nov. 2004.

[15] Y. J. Sung, C. S. Ahn, and Y.-S. Kim, "Size reduction and harmonic suppression of rat-race hybrid coupler using defected ground structure," *IEEE Microw. Wireless Compon. Lett.*, vol. 14, no. 1, pp. 7–9, Jan. 2004.

[16] M.-L. Chuang, "Miniaturized ring coupler of arbitrary reduced size," *IEEE Microw. Wireless Compon. Lett.*, vol. 15, no. 1, pp. 16–18, Jan. 2005.

[17] J.-T. Kuo, J.-S. Wu, and Y.-C. Chiou, "Miniaturized rat race coupler with suppression of spurious passband," *IEEE Microw. Wireless Compon. Lett.*, vol. 17, no. 1, pp. 46–48, Jan. 2007.

[18] C.-L. Hsu, C.-W. Chang, and J.-T. Kuo, "Design of dual-band microstrip rat race coupler with circuit miniaturization," in *IEEE MTT-S Int. Microw. Symp. Dig.*, Honolulu, HI, Jun. 2007, pp. 177–180.

[19] T. Hirota, A. Minakawa, and M. Muraguchi, "Reduced-size branch-line and rat-race hybrids for uniplanar MMIC's," *IEEE Trans. Microw. Theory Tech.*, vol. 38, no. 3, pp. 270–275, Mar. 1990.
[20] IE3D Simulator. Zeland Softw. Inc., Freemont, CA, Jan. 2002.

Ching-Luh Hsu received the M.S. degree in electrical engineering from National Sun Yet-Sen University (NSYSU), Kaohsiung, Taiwan, in 1994, and the Ph.D. degree in communication engineering from National Chiao Tung University (NCTU), Hsinchu, Taiwan, in 2008, respectively.

From 1994 to 1999, he was an RF Engineer with Microelectronic Technology Incorporation (MTI), Hsinchu, Taiwan, where he developed transceivers for point-to-point digital microwaves. In 1999, he joined the faculty of the Department of Electronic Engineering, Ta Hwa Institute of Technology (THIT), Hsinchu, Taiwan, where he is currently an Assistant Professor. His research interests include the design of planar circuits for microwave and millimeter-wave applications.

Jen-Tsai Kuo (S'88–M'92–SM'04) received the Ph.D. degree from the Institute of Electronics, National Chiao Tung University (NCTU), Hsinchu, Taiwan, in 1992.

Since 1984, he has been with the Department of Communication Engineering, NCTU, where he is currently a Professor. From 1995 to 1996, he was a Visiting Scholar with the Electrical Engineering Department, University of California Los Angeles (UCLA). Since February 2007, he been the Secretary General of the NCTU. His research interests include analysis and design of microwave integrated circuits and numerical techniques in electromagnetics.

Dr. Kuo is currently an Editorial Board member of the IEEE TRANSACTIONS ON MICROWAVE THEORY AND TECHNIQUES and the IEEE MICROWAVE AND WIRELESS COMPONENTS LETTERS. He was one of the recipients of the Best Paper Award of the 2002 National Telecommunication Conference, Taiwan, and one of the recipients of the 2007 Asia–Pacific Microwave Conference (APMC) Prize, Bangkok, Thailand. He was also the recipient of the Taiwan Citation Laureate 2006 presented by Thomson Scientific and the 2007 Distinguished Research Award presented by the National Science Council, Taiwan.

Chin-Wei Chang received the B.S. degree in electronic engineering from the National Kaohsiung University of Applied Sciences (NKUAS), Kaohsiung, Taiwan, in 2005, and the M.S. degree in communication engineering from National Chiao Tung University (NCTU), Hsinchu, Taiwan, in 2007, respectively.

He is currently with the Department of Communication Engineering, NCTU. His research interests include the design of RF modules and microwave passive components.